Prediction of Dry-Season Precipitation in Tropical West Africa and Its Relation to Forcing from the Extratropics

PETER KNIPPERTZ

Institute for Atmospheric Physics, Johannes Gutenberg University Mainz, Mainz, Germany

ANDREAS H. FINK

Institute of Geophysics and Meteorology, University of Cologne, Cologne, Germany

ABSTRACT

Precipitation during the boreal winter dry season in tropical West Africa is rare but occasionally results in significant impacts on the local population. The dynamics and predictability of this phenomenon have been studied very little. Here, a statistical evaluation of the climatology, dynamics, and predictions of dry-season wet events is presented for the region 7.5°–15°N, 10°W–10°E. The analysis is based upon Global Precipitation Climatology Project (GPCP) merged satellite–gauge pentad rainfall estimates and 5-day 40-yr European Centre for Medium-Range Weather Forecasts (ECMWF) Re-Analysis (ERA-40) precipitation forecasts, and covers the 23 dry seasons (November–February) during 1979/80–2001/02. Wet events are defined as pentads with an area-averaged precipitation anomaly of more than +200% with respect to the mean seasonal cycle. Composites of the 43 identified events indicate an association with a trough over northwestern Africa, a tropical plume on its eastern side, unusual precipitation at the northern and western fringes of the Sahara, and reduced surface pressure over the Sahara, which allows an inflow of moist southerlies from the Gulf of Guinea to feed the unusual dry-season rainfalls. The results give evidence for a preconditioning by another disturbance about 1 week prior to the precipitation event. The ERA-40 forecasts show a high temporal correlation with observations, a general wet bias, but a somewhat too low number of wet events. With 53% of all identified events correctly forecasted and only 32% of forecasted events not verified, the model shows moderate skill in contrast to the prediction of many other tropical precipitation systems. A separate consideration of hits, misses, and false alarms corroborates the previously proposed hypothesis that a strong extratropical influence enhances the quality of predictions in this region. The results should encourage weather services in West Africa to take advantage of available dry-season precipitation forecasts in terms of the dissemination of early warnings.

1. Introduction

During boreal winter, tropical West Africa is under the influence of dry and often dusty northeasterly harmattan winds from the Sahara. Regular rainfalls are absent, except for the coastal strip between the Grain Coast area of western Africa and the Niger River delta (e.g., Buckle 1996). Occasional dry-season precipitation events in the Soudano–Sahelian zone of West Africa have been termed mango or heug rains in the western part and are often related to upper-level disturbances intruding from the extratropical North Atlantic into the tropics (Seck 1962; Griffiths 1972; Borgne 1979; Gaye et al. 1994; Issar 1995; Buckle 1996; Leroux 2001). Recently, Knippertz and Fink 2008a, hereafter KF08) documented a case of an unusual northward penetration of the rain zone into the countries of Ghana, Togo, Benin, and Nigeria in January 2004. Despite their rare occurrence, dry-season wet events can have substantial impacts on the local hydrology and human activities reaching from greening pastures to flooding and rotting harvests (Knippertz and Martin 2005; Fall et al. 2007; KF08). KF08 proposed a close link of the unusual tropical rainfalls to the synoptic evolution in the extratropics. They show that extratropical disturbances penetrating into low latitudes support a diabatic pressure fall over West Africa through the anomalous radiative warming under a diagonal cloud

Corresponding author address: Peter Knippertz, Institute for Climate and Atmospheric Science, School of Earth and Environment, University of Leeds, Leeds, LS2 9JT, United Kingdom.
E-mail: p.knippertz@leeds.ac.uk

band on the eastern flank of a first trough, often referred to as a tropical plume (TP; see Knippertz 2005), and a dynamical pressure fall through subsidence and warm advection associated with a subsequent second upper-level trough. As a consequence of the reduced surface pressure, moist monsoon air from the Gulf of Guinea penetrates inland and allows the formation of deep moist convection and heavy precipitation. In the case discussed by KF08, extreme precipitation also occurred in subtropical northwest Africa to the east of the second trough.

Based on this case study, KF08 hypothesized that the strong extratropical influences may imply a comparably good predictability of such events that would allow a timely warning of the population and therefore a mitigation of detrimental impacts as well as an exploitation of beneficial effects. To test this hypothesis, the present study gives a statistical evaluation of boreal winter precipitation forecasts made by the 40-yr European Centre for Medium-Range Weather Forecasts (ECMWF) Re-Analysis project (ERA-40; Uppala et al. 2005). Only the geostationary satellite period from 1979 to 2002, usually regarded as the more reliable part of the dataset for climatological analyses (Kållberg et al. 2005), will be considered. The objectives of this study are (a) to identify episodes of a temporary northward extension of the ITCZ rainfall belt onto the West African continent during the dry season (November–February), (b) to understand the dynamics of the rainfall generation including the role of the extratropics, (c) to evaluate the ability of a state-of-the-art numerical weather prediction (NWP) model to forecast such events, and (d) to investigate in what way the degree of extratropical influence is related to forecast skill. The remainder of the paper is structured as follows. Section 2 provides information on the employed observational and forecast data. Section 3 contains an exemplary case study. Section 4 describes the identification of dry-season wet events and their climatology, while section 5 evaluates ERA-40 forecasts of these events. Section 6 contains a detailed analysis of the dynamics including a differentiation between successful and unsuccessful forecasts. The most important results are summarized and discussed in section 7 together with a compilation of open research issues.

2. Data

a. Precipitation observations

The main observational dataset used in this study is a merged satellite–gauge product provided by the Global Precipitation Climatology Project (GPCP). This dataset includes microwave precipitation estimates based on Special Sensor Microwave Imager (SSM/I) data from the polar-orbiting Defense Meteorological Satellite Program (DMSP) satellites and infrared (IR) precipitation estimates from geostationary and polar-orbiting satellites. Additional low-earth orbit estimates include the Atmospheric Infrared Sounder (AIRS) data from the National Aeronautics and Space Administration (NASA) *Aqua* satellite, and Television Infrared Observation Satellite Program (TIROS) Operational Vertical Sounder (TOVS) and outgoing longwave radiation precipitation index (OPI) data from the National Oceanic and Atmospheric Administration (NOAA) series of satellites. The gauge data are assembled and analyzed by the Global Precipitation Climatology Centre (GPCC) of the German Weather Service (Deutscher Wetterdienst, DWD) and by the Climate Prediction Center of NOAA. The blending procedure is described in Adler et al. (2003). Here, the pentad product that provides precipitation estimates on a 2.5° grid over the entire globe at 5-day intervals for the period January 1979–present (Xie et al. 2003) is used. For leap years the pentad period starting on 25 February covers 6 days. The data were downloaded in network common data form (NetCDF) from the World Wide Web (WWW; http://www.jisao.washington.edu/data_sets/ gpcp/daily/pentad.html). A comparison of GPCP data with Climate Prediction Center Merged Analysis of Precipitation (CMAP) data on a monthly basis revealed the good performance of the GPCP data in regions with low gauge density such as West Africa (Yin et al. 2004).

For the study of some cases occurring after 1998, the Tropical Rainfall Measuring Mission (TRMM) and other data precipitation dataset (3B42 V6; Huffman et al. 2007) at a much higher spatial resolution of 0.25° is additionally used for comparison. These data are 3-hourly combined microwave–IR estimates (with gauge adjustment) and were downloaded from the NASA Web site (http://disc2.nascom.nasa.gov/Giovanni/tovas/). The gauge data employed here are standard surface synoptic observations (SYNOPs) from the archive of the DWD and the Global Summary of the Day (GSOD) data provided by the National Climatic Data Center (NCDC; ftp.ncdc.noaa.gov/pub/data/gsod/).

b. ECMWF and CLAUS data

The precipitation forecasts evaluated in this study come from the ERA-40 reanalysis project by the ECMWF (Uppala et al. 2005). Accumulated total precipitation (i.e., convective plus large scale) from 120-h forecasts with the ERA-40 model version T159L60 started at 0000 UTC of the first day of each of the GPCP pentads (see section 2a) is considered, which results in a perfect temporal match. Note that this resolution is considerably coarser

than the current model version T799L91. The data were retrieved from the ECMWF archive at 1° × 1° latitude–longitude horizontal resolution and then interpolated onto the GPCP 2.5° × 2.5° grid using a bicubic interpolation routine contained in the Climate Data Operators software package developed at the Max Planck Institute for Meteorology in Hamburg, Germany (information online at http://www.mpimet.mpg.de/fileadmin/software/cdo/). The interpolation occasionally generates spurious negative rainfalls that were set to zero.

For the analysis of the large-scale atmospheric circulation and forecast errors in section 6, ERA-40 reanalysis and forecast fields of mean sea level pressure (MSLP), geopotential height at 500 hPa (Z500), and 2-m dewpoint temperature (TD2M) on a 1° × 1° latitude–longitude grid were considered that are available every 6 h. Note that the TD2M fields were not directly produced by the primary three-dimensional variational data assimilation (3DVAR) analysis but by an optimum interpolation of measurements and are therefore relatively slightly influenced by the ECMWF model (see chapter 3d in Uppala et al. 2005). As a climatological background, ERA-40 long-term monthly means of 1200 UTC Z500, MSLP, and TD2M were computed for the period 1979–2001. For the analysis of clouds, thermal IR window (10.5–12.5 μm) brightness temperatures (BTs) provided by the Cloud Archive User Service (CLAUS) were downloaded from the British Atmospheric Data Centre (BADC; http://badc.nerc.ac.uk/data/claus). CLAUS merges information from several geostationary and polar-orbiting satellites [e.g., NOAA, Geostationary Operational Environmental Satellite (GOES), Meteosat, and Geostationary Meteorological Satellite (GMS)] into a homogeneous global dataset (Hodges et al. 2000). The horizontal resolution of this dataset is 0.5° and BT fields are available every 3 h for the period July 1983 to the present. Unfortunately, the first four dry seasons considered for the GPCP analysis are not covered by CLAUS, slightly reducing the numbers of cases available for the composite analysis in section 6.

3. An example case study

As an introduction to the problem, a case study of an unusual dry-season rainfall event is presented. Figures 1a and 1b show the accumulated precipitation for the 15–19 February 1999 pentad from the GPCP and TRMM datasets together with station observations. These data clearly indicate that the precipitation zone, usually restricted to the near-equatorial Atlantic Ocean and Gulf of Guinea during the dry season (e.g., Fig. 11 in Xie and Arkin 1997), reached unusually far into the study area over the West African continent marked with black
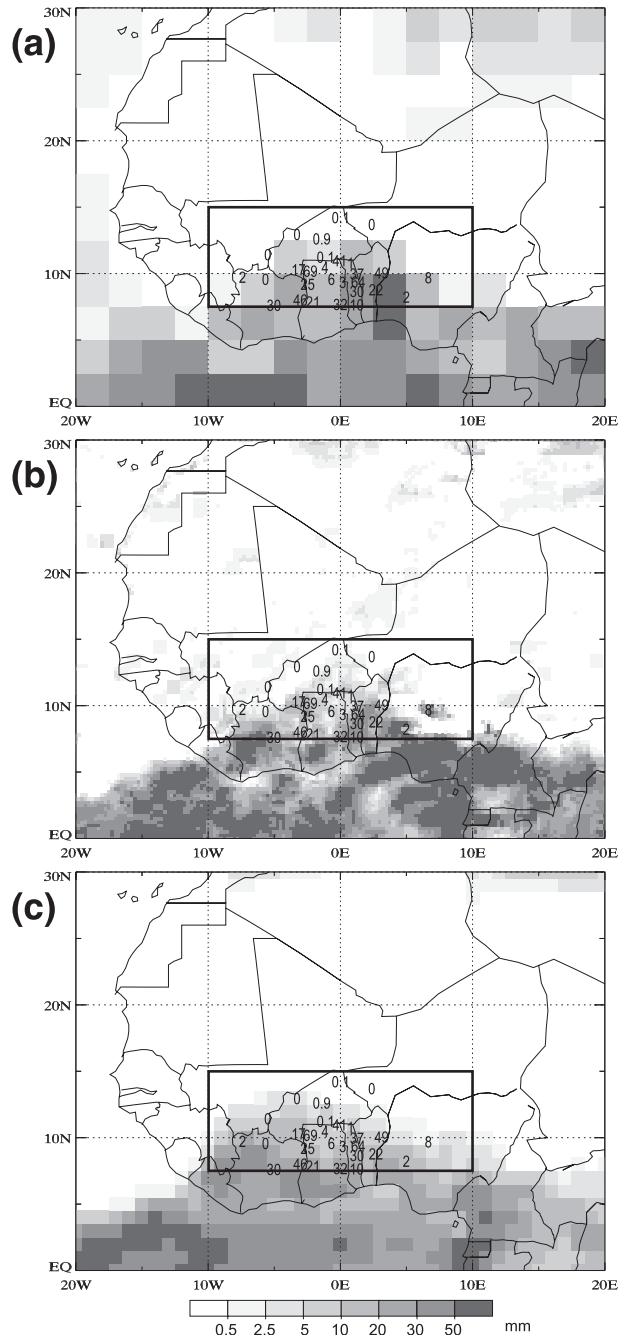

FIG. 1. 5-day accumulated precipitation during the pentad 15–19 Feb 1999 (in mm) from (a) GPCP, (b) TRMM, and (c) ERA-40 forecast data. Observations from selected rain gauges are indicated as numbers, with 0 indicating traces of rain. Black boxes mark the study area.

boxes in Fig. 1. The coarse-resolution GPCP data (Fig. 1a) show a maximum grid-box value in excess of 50 mm over western Nigeria and even some precipitation to the north of 10°N. The high-resolution TRMM data contain much greater detail and indicate regions with highest
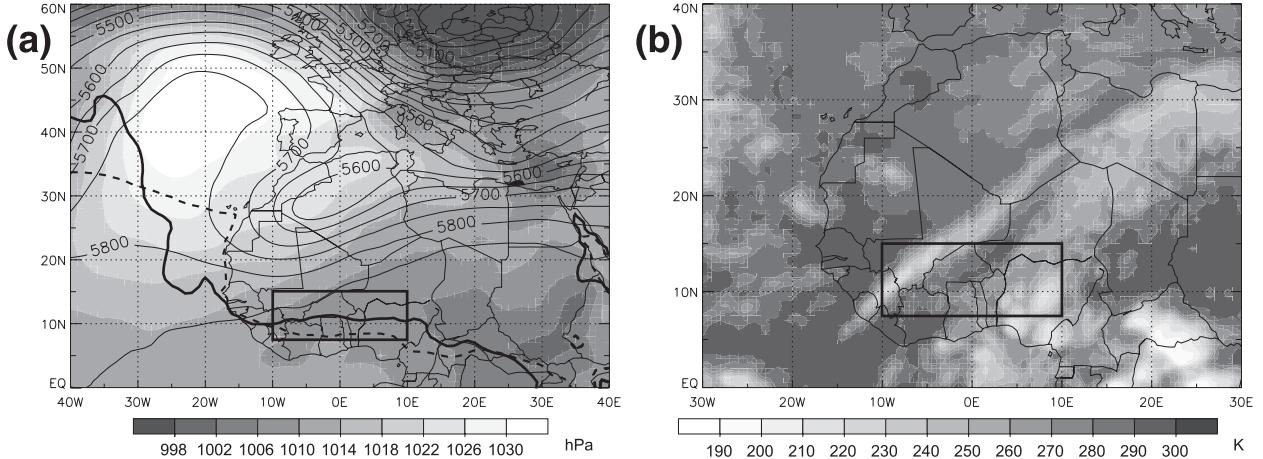
FIG. 2. (a) Z500 (contours every 50 gpm), MSLP (shading), and 14°C contour of TD2M (thick solid line) at 1200 UTC 17 Feb 1999. The dashed line shows the 1979–2002 February average of the latter contour as a reference. (b) The CLAUS IR brightness temperatures at 2100 UTC on this day. Black boxes mark the study area.

rainfalls over central Ivory Coast and western Nigeria, also with amounts exceeding 50 mm (Fig. 1b). The selected station observations confirm these unusual rainfalls, with values ranging from 46 mm at Bondoukou (8.05°N, 2.78°W) and 44 mm at Parakou (9.35°N, 2.62E) to traces as far north as Dori (14.03°N, 0.03°W). The recorded amount at Parakou corresponds to almost 5 times the 1961–1990 February average of 9 mm. Such amounts substantially affect the local hydrology and vegetation as exemplified in KF08. Unfortunately, the few available reports from the Nigerian synoptic network do not confirm the maxima in the satellite estimates. Interestingly, both datasets indicate scattered patches of light rain over the Sahara. The synoptic data indicate that the precipitation fell during the first 4 days of the pentad, mainly during the afternoon and evening hours, suggesting a triggering of convection by daytime heating. The corresponding 5-day precipitation forecast from the ERA-40 data reproduces the unusual shift of the precipitation zone into the continent well, while some of the fine structure evident from the TRMM and station data is missing (Fig. 1c). This suggests that the ECMWF model is capable of simulating the changes in the large-scale circulation that allow convection to form farther north than usual but struggles to correctly reproduce the details of the convective dynamics. Such a forecast is nevertheless of great value to the local population as discussed in the introduction.

The unusual rainfalls are associated with a very pronounced, strongly tilted upper-level trough across northwestern Africa downstream of an equally pronounced upper ridge as indicated by Z500 at 1200 UTC 17 February 1999 (Fig. 2a). MSLP is reduced over a large area to the southeast of the trough axis, allowing

low-level southerly moisture advection into the continent. This is clearly indicated by the northward shift of the 14°C contour of TD2M (thick lines in Fig. 2a) that is often used as an indicator for the position of the intertropical discontinuity (ITD), the boundary between dry Saharan and moist tropical air over West Africa (Buckle 1996). A maximum MSLP anomaly of −8 hPa with respect to the long-term February mean is analyzed over northern Niger near 20°N, 10°E (not shown). Nine hours later, CLAUS BTs show a TP along the southeastern flank of the trough (Fig. 2b). While the straight cloud band over Mali caused rather little precipitation, some rainfall was associated with the widespread deep convection over Nigeria. It is conceivable that low inertial stability at the anticyclonic flank of the subtropical jet streak accompanying the upper trough has provided good outflow conditions for convection (Mecikalski and Tripoli 1998; Knippertz 2005). The situation resembles the dry-season precipitation case discussed in KF08, who suggested a relation between the pressure fall over West Africa and the combined affects of warm advection and an enhanced greenhouse effect under the TP. The Z500, MSLP, TD2M, and CLAUS BT data will be used for the composite analysis of the dynamics of dry-season rainfalls in section 6.

4. Climatology of dry-season precipitation events

In this section the method of obtaining a climatology of dry-season precipitation events is described, including an explanation of the identification algorithm and the motivation behind the chosen thresholds in section 4a. This algorithm is then applied to the entire GPCP
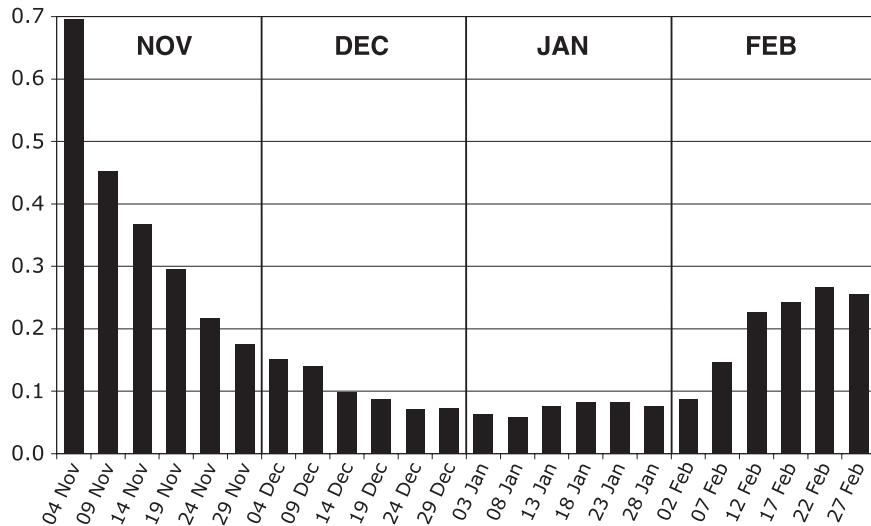
FIG. 3. Mean pentad precipitation (mm day^{-1}) over the area 7.5°–15°N, 10°W–10°E during the West African dry season of 2 November–1 March based upon GPCP pentad precipitation estimates of the 23 dry seasons from 1979/80 to 2001/02. The dates along the abscissa give the center day of the respective pentad. Months are defined as in Table 1.

pentad dataset in section 4b and to the ERA-40 forecasts in section 5. In section 4c some remarkable events identified with the algorithm will be discussed.

a. Identification

The first step of the identification procedure is to calculate area averages of precipitation over the box indicated in Figs. 1 and 2 spanning 7.5°–15°N, 10°W–10°E. For the GPCP pentad data this corresponds to eight grid boxes in the zonal and three grid boxes in the meridional directions, that is, 24 grid boxes in total. The second step is to estimate a climatological background for the computation of anomalies. To get a smooth annual cycle from the 23 yr of GPCP data, a three-pentad (= 15 days) sliding window is used; that is, the climatological mean for a given pentad is calculated from 69 different pentad values. The investigations are restricted to the main dry season spanning the 24 pentads from 2–6 November to 25 February–1 March. During this period, the precipitation rates stay below 0.7 mm day^{-1}, typical of the dry season (Fig. 3). Highest values are reached for the first pentad in early November and then precipitation rates slowly decrease to values below 0.1 mm day^{-1} from mid-December to the beginning of February, followed by a rather abrupt increase to values around 0.25 mm day^{-1}. The standard deviations for these 15-day means are of the same magnitude or larger than the mean values themselves, indicating substantial interannual variability.

The third step in the identification routine is to calculate anomalies with respect to the mean annual cycle

shown in Fig. 3. These anomalies can be expressed in absolute numbers, that is, in units of millimeters per day, or in a relative sense, that is, in percent with respect to the pertinent climatological pentad mean. This way an anomaly of −100% corresponds to no precipitation at all, while for example an anomaly of +200% means 3 times the average precipitation. As an example, Fig. 4 shows the anomaly values in both absolute and relative numbers for the 24 pentads of the dry season 1998/99. Many pentads show negative anomalies, some even close to −100%, indicating basically dry pentads. The fact that the absolute anomalies decrease for a given relative anomaly toward the middle of the plot is a result of the annual cycle (Fig. 3). Only eight pentads have positive anomalies, demonstrating the episodic nature of dry-season rainfalls. The most prominent are pentad 8 with +0.26 mm day^{-1} (i.e., +187%), pentad 14 with +0.14 mm day^{-1} (i.e., +241%), and pentad 22 with +1.3 mm day^{-1} (i.e., +538%). Pentad 22, during which more than 6 times more precipitation fell than is usual, is the example case presented in section 3. The area-average accumulated rainfall during this pentad is 7.7 mm, but Figs. 1a and 1b show that locally amounts on the order of 50 mm and more were observed. The last step is the definition of a significant dry-season wet event. The identification threshold was arbitrarily set to +200% (i.e., 3 times the mean rainfall). In Fig. 4 only the two pentads, 6–10 January and 15–19 February 1999, fulfill this criterion. A relative anomaly threshold is preferred to an absolute one to account for the annual cycle. In addition, a stronger tropical influence on precipitation is expected
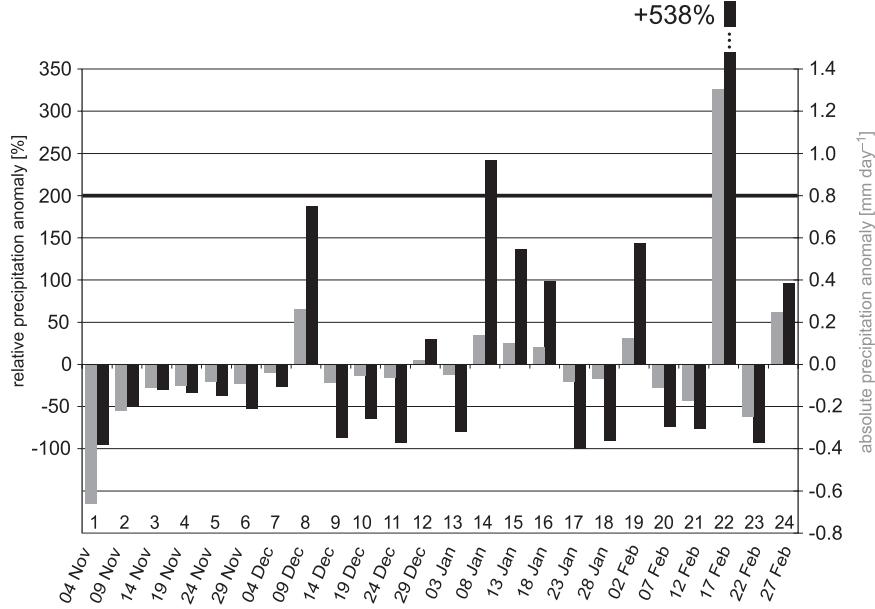
FIG. 4. Pentad precipitation anomalies over the area 7.5°–15°N, 10°W–10°E during the West African dry season of 2 Nov 1998–1 Mar 1999. Anomalies were calculated with respect to the mean pentad values displayed in Fig. 3 and expressed in mm day^{-1} (gray bars, right ordinate) and in % (black bars, left ordinate), respectively. The dates along the abscissa give the center day of the respective pentad, which are numbered serially for reference in the text.

in November and therefore the authors prefer to consider only the strongest events in this month, for which an influence of the extratropical circulation can be assumed. The obvious disadvantage of this approach is that the impact on the hydrology can differ for a typical January compared to a typical November event.

b. Climatology

When applying the +200% anomaly criterion to the 23 dry seasons 1979/80 to 2001/02, in total 43 wet events are obtained, or 1.87 per year. In other words, 7.8% of all pentads (about every 13th pentad) are wet. Figure 5 shows a time series of the number of wet pentads per
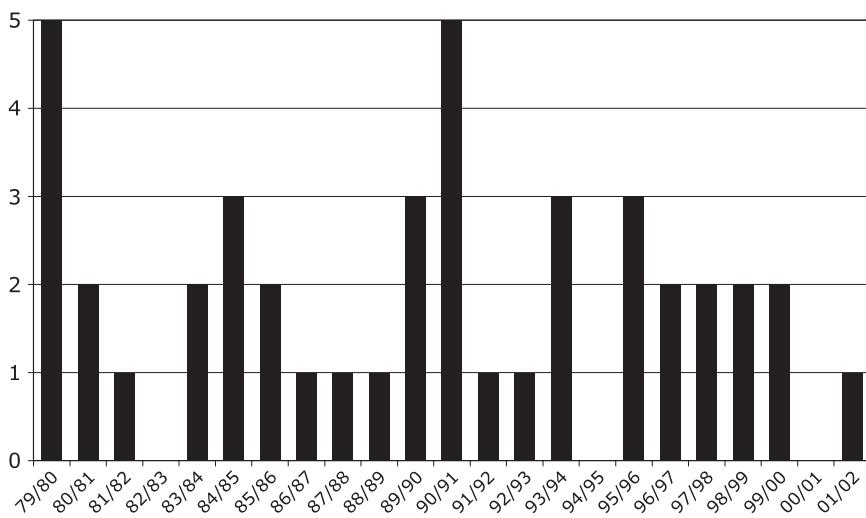

FIG. 5. Number of precipitation events for the 23 dry seasons from 1979/80 to 2001/02 as identified from GPCP pentad data using the routine described in section 4a.

TABLE 1. Monthly statistics of mean precipitation and number of dry-season precipitation events for two different thresholds. Data are based on the GPCP pentad precipitation estimates for the 23 dry seasons 1979/80–2001/02. For details on the identification of events, see section 4a.

Month	Period	Mean precipitation (mm day^{-1})	No. of wet events (>200%)	No. of wet events (>300%)
Nov	2 Nov–1 Dec	0.33	11	5
Dec	2–31 Dec	0.11	13	9
Jan	1–30 Jan	0.07	13	5
Feb	31 Jan–1 Mar	0.21	6	5
All	2 Nov–1 Mar	0.18	43	24

FIG. 6. Composited GPCP precipitation over all 43 wet events identified in section 4, in millimeters per pentad. A black box marks the study area.

season, which varies between zero in 1982/83, 1994/95, and 2000/01 and five in 1979/80 and 1990/91. There are 7 yr with, respectively, one and two events. There is no obvious trend in this time series. Table 1 shows the average monthly distribution of wet events. Here a "month" consists of six pentads regardless of the actual length of the calendar month (second column in Table 1). With 13 events each, most events occur in December and January, when the mean precipitation and therefore the absolute exceedence thresholds are lowest. However, the fact that there are substantially more events in the relatively wet November than in February indicates that the number of wet events in this relative sense is not simply anticorrelated with the absolute value of the exceedence threshold. Possibly, the substantial differences in soil moisture and vegetation at the beginning and end of the dry season affect inter alia vertical stability and moisture availability. The number of identified events is, of course, sensitive to the arbitrarily chosen threshold. With +300% instead of +200%, the total number is reduced to only 24 events with a slightly flatter annual cycle (Table 1).

Figure 6 shows a composite of GPCP precipitation for all 43 identified dry-season wet events. The highest absolute values occur in the Atlantic ITCZ and close to southern Italy. Within the study region (marked by a black box in Fig. 6), there is a distinct south–north decrease in rainfall, but also a west–east gradient, leading to a precipitation maximum over the Guinean Highlands and leaving the five grid boxes over northern Burkina Faso and southern Niger almost dry. Therefore, restricting the study region to the southern two rows of grid boxes spanning 7.5°–12.5°N would not have a very large effect on the event detection (not shown). There are five cases in which restricting the domain will increase the anomaly from just below the threshold of +200% to just above it. On the other hand, there are three cases in which rainfalls between 12.5° and 15°N contribute substantial amounts to the area average,
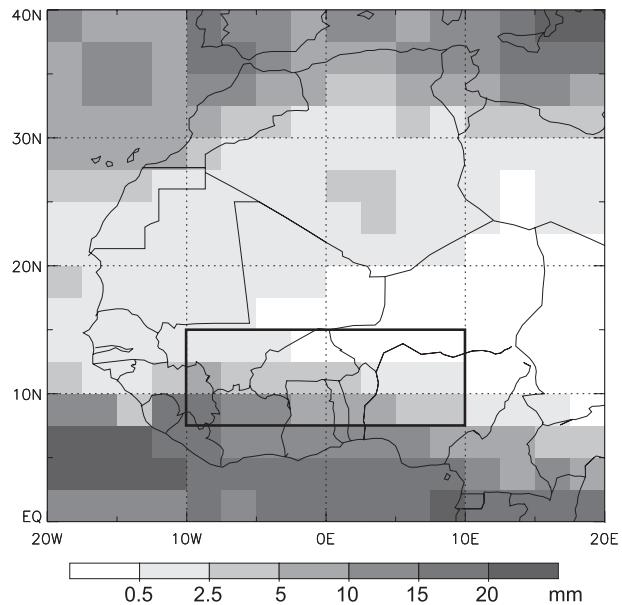
most notably during the pentad 21–25 January 1992, when a large precipitation band reached all the way across the Sahara into the Sahel. Over the entire time period the correlation between precipitation over the whole region and just the southern two rows of grid boxes is greater than 0.99. Interestingly, the composite in Fig. 6 indicates both a northward extension of the tropical precipitation zone and a southward extension of the subtropical rainfalls affecting large parts of the western and northern Sahara. This pattern is consistent with the case shown in Fig. 1 and the one analyzed by KF08, and corroborates a dynamical linkage between remote wintertime precipitation events to the south and north of the Sahara.

c. Remarkable events

The algorithm presented above identifies five events with anomalies of more than 1000%, all during the driest months of December and January. These include 27–31 December 1989, 1–5 January 2000, and 6–10 January 2002. In the former two cases, the available station reports indicate widespread, moderate to abundant rainfall amounts between 10 and 47 mm in the west-central part of the study region. The latter event also brought record-breaking precipitation in excess of 50 mm to parts of Senegal and Mauritania with harmful impacts on the local population (Knippertz and Martin 2005; Fall et al. 2007; Meier and Knippertz 2009). Station reports in the investigation area during this event peaked at 23 mm in Bouake (7.73°N, 5.06°W) and
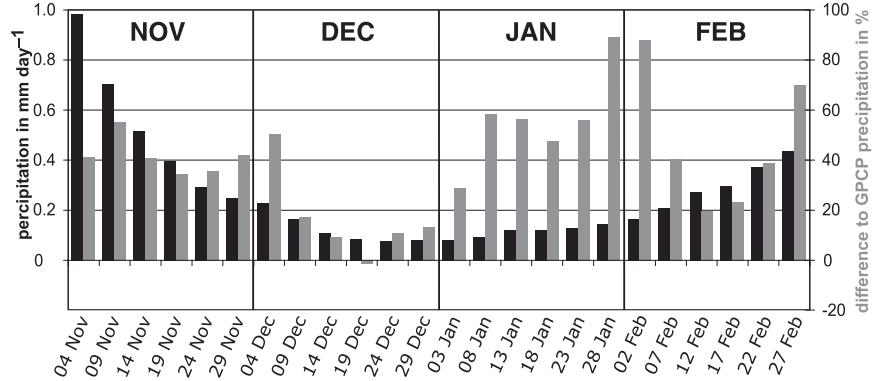
FIG. 7. Black bars show the mean annual cycle of precipitation as in Fig. 3 but based upon 5-day ERA-40 precipitation forecasts. The gray bars indicate the differences between the ERA-40 and GPCP data in %.

at 20 mm in Save (8.03°N, 2.48°E). Also quite unusual is the three-pentad period 12–27 December 1990 with positive anomalies of 1082%, 212%, and 1482% corresponding to an accumulated area-averaged precipitation of 12.7 mm (almost 4 times the December average; see Table 1). At Bondoukou (8.05°N, 5.06°W) the December sum of 54 mm constitutes more than 4 times the 1961–90 Climatological Normal (CLINO) rainfall of 11 mm. This event is related to a repeated regeneration of a distinct trough over northern Africa. There are five more events with anomalies of more than +500%, one of which is the case presented in section 3. The others are 16–20 January 1980, 15–19 February 1982, 21–25 January 1992, and 10–14 February 1996. In January 1980, 81 mm fell at Bondoukou, which constitutes about 10 times the average January rainfall of the 1961–90 period. Bouake recorded 87 mm in February 1982. As shown in Knippertz and Martin (2005), and KF08 for January, values in excess of 100 mm per event are possible and cause local flooding at the peak of the dry season.

5. Forecast evaluation

a. Climatology

In this section, the GPCP results from section 4 are compared to 5-day ERA-40 forecasts. For an optimal comparison, the exact same 23 yr and 24 pentads per year (i.e., 552 pentads) are used, with forecasts being started at 0000 UTC on the first day of the respective pentads. After applying the area average and the three-pentad running-window time average described in section 4a to the forecast data, a mean seasonal cycle analogous to Fig. 3 is obtained (black bars in Fig. 7). The gray bars in Fig. 7 show the differences from GPCP in percent, indicating a marked wet bias of the ECMWF model with only one pentad showing an underestimation

(cf. Fig. 6 in Hagemann et al. 2005). Absolute differences can be as high as 0.29 mm day^{-1} with an average over all 24 pentads of 0.08 mm day^{-1} (not shown). In a relative sense the overestimation varies from −1% to 89%, with the largest values in January and an average of 40% (Fig. 7).

Despite this wet bias, the temporal accordance between the two datasets is rather good. Figure 8 shows scatterplots relating the area-averaged and grid-box maximum precipitation amounts of all 552 pentads from GPCP and ERA-40. The area averages in both datasets cover the range from 0 to ~3.2 mm day^{-1}, and most data points are relatively close to the diagonal without any extreme outliers (Fig. 8a). In accordance with Fig. 7, there is a general tendency of slightly higher ERA-40 values. The linear correlation coefficient r equals 0.77, indicating that the ECMWF model is able to predict more than half of the variability in this parameter. Since the data do not have a Gaussian distribution, a rank correlation is performed that basically confirms this positive result (Fig. 8b). The data points scatter uniformly around the diagonal with similar numbers of occurrences of no precipitation in both datasets. The correlation coefficient of 0.75 is only slightly lower than in Fig. 8a. For grid-box maxima the correspondence between the two datasets is satisfactory as well (Fig. 8c). Both datasets span the range between 0 and ~15 mm day^{-1} and again extreme outliers are rare, even for large rainfall amounts. The linear correlation coefficient still reaches 0.59 for this parameter.

b. Events

To examine the ability of the ECMWF model to reproduce dry-season wet events, the routine described in section 4a was applied to ERA-40 forecasts for the same 552 pentads. Due to the positive bias found in
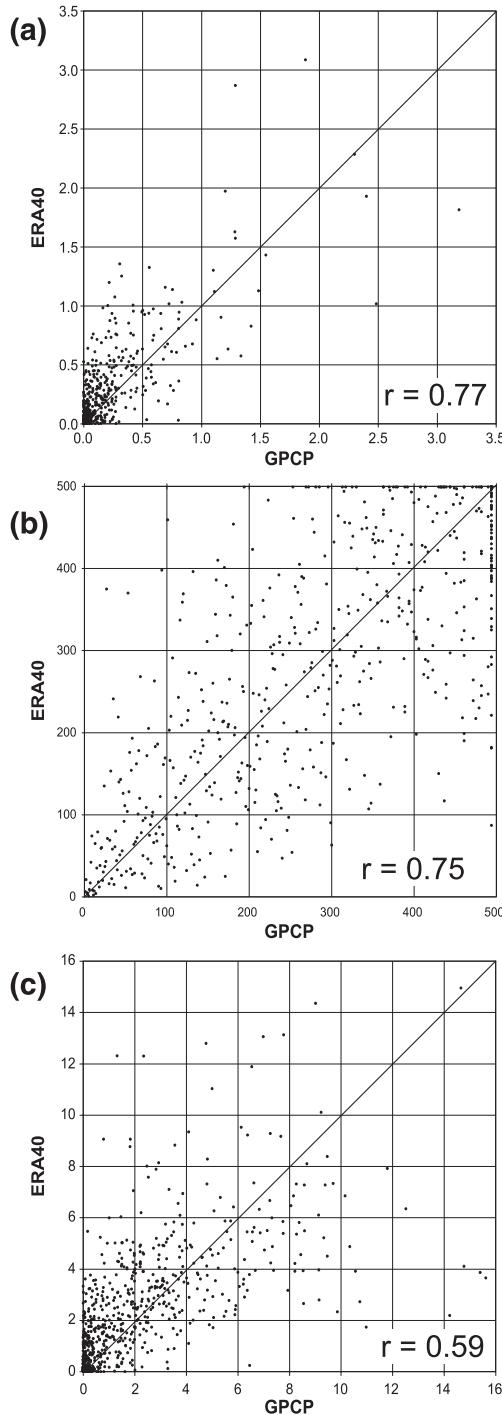
FIG. 8. Scatterplots relating pentad precipitation data from GPCP (abscissas) to ERA-40 5-day forecasts (ordinates) for the 552 pentads from 2 Nov to 1 March 1979/80–2001/02. (a) Area averages for 7.5°–15°N, 10°W–10°E (mm day⁻¹). (b) Ranking of the area averages shown in (a). Rank 494 in the GPCP data and rank 499 in the ERA-40 data correspond to zero precipitation. (c) As in (a) but for the 2.5° × 2.5° gridbox maxima. The linear correlation coefficient r is given in each panel. All correlations are significant at the 99.9% significance level.

section 5a, the employed identification threshold corresponds to a +200% anomaly with respect to the ERA-40 forecasts and not with respect to the GPCP data. This limits the comparability between the two datasets in an absolute sense, but is unavoidable in order to obtain similar numbers of events. A sensitivity test using the GPCP thresholds resulted in an undesirable almost doubling of wet events and 3.5 times more false alarms. Using the ERA-40 thresholds, the total number of wet events in the forecasts is 34 and thus significantly smaller than in the GPCP data. This result reflects the often-documented tendency of NWP models to generate too much light precipitation while missing out on higher intensities (e.g., Frei et al. 2003). The seasonal distribution is similar to GPCP with most events in January (11) and December (9), and lesser numbers of events in November (6) and February (8) (for a definition of the periods and the corresponding GPCP results, see Table 1). The latter number indicates a tendency to overpredict February events. The number of events per season varies between zero (6 yr) and six events in 1990/91 (not shown). The linear correlation with the GPCP time series in Fig. 5 is 0.64. There is no obvious trend or clustering of events, suggesting that changes in data availability during the ERA-40 period did not have significant impacts.

Table 2 shows an evaluation of the ERA-40 forecasts of wet events based upon the number of hits (h), misses (m), false alarms (f), and correct negatives (z) for the whole study period and for two subperiods, that is, the first 11 and the last 12 yr. The first two columns indicate that 23 out of the 43 events identified in section 4 are correctly forecasted, resulting in a hit rate (H) of 0.53 (for a definition of score indices, refer to Table 2 caption). Eleven out of the 34 events in the ERA-40 forecasts did not verify in the GPCP data, leading to a false alarm rate (F) of 0.02 and a false alarm ratio (FAR) of 0.32. Here, F is the proportion of nonoccurrences that were incorrectly forecasted, whereas FAR is the proportion of forecasts of occurrence that did not verify. For a rare event like a dry-season rainfall, FAR is of more interest as an operational application. Too few events in the ERA-40 forecasts result in a frequency bias (B) of 0.79. A substantially larger H than F and a Heidke skill score (HSS) of 0.56 (an HSS of zero means no skill and an HSS of one is a perfect forecast) indicate a moderate level of skill in the ERA-40 forecasts. FAR and H vary rather little over the 4 months under consideration with an exception in February when FAR reaches 0.63 (not shown). Consistently, February is the only month for which more events are predicted than observed (B of 1.33). In contrast, a relatively high m and a low B of 0.55 characterize November. When using a threshold of 300% as in Table 1, H and HSS decrease to

TABLE 2. Quality of ERA-40 forecasts of dry-season wet events evaluated with GPCP data. The rows give the numbers of hits (h), misses (m), false alarms (f), correct negatives (z), and total number of dates (n) for the whole study period and two subperiods. The definitions of the indices used are (see Mason 2003 for more details): frequency bias, $B = (h + f)/(h + m)$; hit rate, $H = h/(h + m)$; false alarm rate, $F = f/(f + z)$; FAR = $f/(h+f)$; and HSS = $(PC - E)/(1 - E)$, where PC is the proportion correct [$PC = (h + z)/n$] and E is the proportion of forecasts that would have been correct, if forecasts and observations were independent: $E = 1/n^2[(h + m)(h + f) + (z + m)(z + f)]$. The HSS varies between 0 (no skill) and 1 (perfect forecast).

	1979/80–2001/02	1979/80–1989/90	1990/91–2001/02
h	23	8	15
m	20	13	7
f	11	4	7
z	498	239	259
n	552	264	288
B	0.79	0.57	1.00
H	0.53	0.38	0.68
F	0.02	0.02	0.03
FAR	0.32	0.33	0.32
HSS	0.57	0.45	0.66

0.46 and 0.48, respectively, while FAR increases to 0.45 (not shown).

Comparing the two right-hand-side columns in Table 2 indicates an improvement in forecast skill during the last 12 yr of the study period. While FAR and F do not change much, H increases from 0.38 to 0.68. The latter period reveals an HSS of 0.66 and a "perfect" B of 1 (22 events in both datasets). Most likely, the increasing availability of more refined satellite information and thus better initial conditions have contributed to this improvement, although natural variations could well be responsible for this behavior as well. In a pilot study to the work presented here, operational ECMWF precipitation forecasts were considered instead of ERA-40 forecasts, revealing a dramatic overprediction of wet events during the 1980s and early 1990s and an increase in skill after 1997/98 (Knippertz and Fink 2008b). This progress is presumably due to both better data availability and improvements to the model and data assimilation system, in particular the change from optimum interpolation to 3DVAR in 1996 and to 4DVAR techniques in 1997.

The overall satisfactory performance of the ERA-40 forecasts at the "extreme" end of the precipitation distribution in a tropical region was not to be expected a priori and corroborates the speculation by KF08 that dry-season precipitation in West Africa might in fact be better predicted by state-of-the-art NWP models than the more intense summer precipitation when extratropical influences are weak. In this evaluation it should be kept in mind that the "truth" represented here by the

GPCP data also has a certain uncertainty range in a region with spatially inhomogeneous rainfalls and observations sparsely distributed in time and space. One example that illustrates the occasional disagreement between different data sources is the case study presented in section 3 (Figs. 1a and 1b).

c. Example cases

In this section, example cases of hits, misses, and false alarms will be discussed. The 10 most extreme positive anomalies in the GPCP data with values of more than +500% (see section 4c) are all correctly identified as wet events by ERA-40, even though the anomalies are mostly not as high as in the observations. In particular the example case described in section 3, the extreme event in January 2002 discussed among others by Knippertz and Martin (2005), and the series of three wet events in December 1990 are well reproduced. Most of the 20 misses have anomalies rather close to the required +200% in the ERA-40 forecast data, but there are also six major forecast busts with negative precipitation anomalies. These cases occur in the driest part of the year between 2 December and 4 February (Fig. 3). Absolute numbers range from 0.2 to 0.8 mm day^{-1} in GPCP and from 0.03 to 0.13 mm day^{-1} in the corresponding ERA-40 data. The most extreme case is the 2–6 December 1997 pentad, when GPCP shows an anomaly of +432% with widespread precipitation over Nigeria and Benin (Fig. 9a), while ERA-40 forecasts concentrate precipitation over the western Gulf of Guinea (Fig. 9b) associated with an anomaly of −86% in the study area. For this period there are no station data available to confirm the precipitation in the southeastern part of the study region. The fact that the large-scale situation is characterized by an upper-level trough over northwestern Africa, reduced MSLP over the western Sahara accompanied by a slight northward shift of low-level moisture over the western part of the study region only (Fig. 9c), and a TP reaching from Ivory Coast to the eastern Mediterranean (Fig. 9d) calls the GPCP estimates into some doubt. A similar situation with anomalies of +295% and −88%, respectively, occurs during 26–30 January 1981.

The worst false alarm occurs during 6–10 January 1997, when ERA-40 forecasts an anomaly of more than +400%, while the GPCP indicates no precipitation at all (i.e., anomaly of −100%). All available observations show rainfalls being largely restricted to the Gulf of Guinea (Fig. 10a), while the ECMWF model shifts the rain inland over almost the entire width of the study area (Fig. 10b). The observed absence of precipitation is consistent with comparably weak troughs in the subtropics (Fig. 10c) and few clouds over the study region
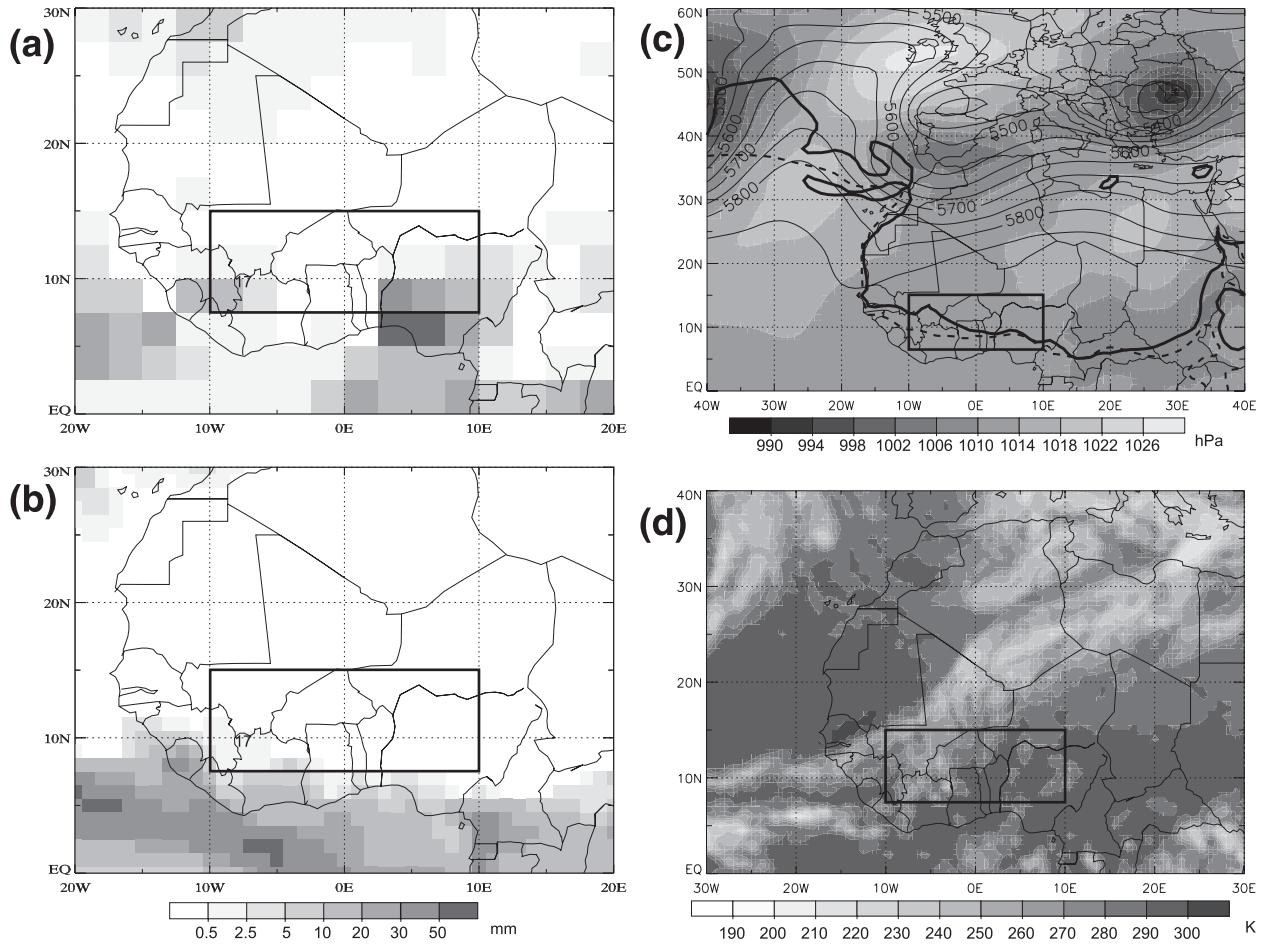
FIG. 9. Example of an extreme forecast miss. The 5-day accumulated precipitation during the pentad 2–6 Dec 1997 (mm) from (a) ERA-40 forecast data and (b) GPCP. Only the synoptic station Odienne reported precipitation during this period. (c) Analyzed Z500 (contours every 50 gpm), MSLP (shading), and 14°C contour of TD2M (thick solid line) at 1200 UTC 4 Dec 1997. The dashed line shows the 1979–2001 December average of the latter contour as a reference. (d) CLAUS IR BTs at 2100 UTC 4 Dec 1997. Black boxes mark the study area.

(Fig. 10d). The analyzed low-level moisture field, however, does show a northward shift, indicating that the model is either too moist or triggers precipitation too easily. Similar patterns are responsible for the misforecasts during 5–9 February 1986 and 7–11 December 1988, while the false alarm of 16–20 January 1996 reveals a too strong penetration only in the western half of the domain. This analysis suggests that the overprediction of rainfall in the false alarm cases in the ECMWF model is not the result of one or two unrealistic ''grid-point storms'' but is rather due to regional-scale problems.

6. Dynamics

In this section the dynamics of the wet events identified and investigated in the previous sections will be examined with a focus on three issues: 1) How closely does the typical evolution of a wet event agree with the case-study results of KF08 (see section 1)? This question is addressed in section 6a on the basis of composites of ERA-40 reanalysis fields and CLAUS BTs for all 43 events. 2) To what extent do the details of the dynamics influence the quality of the ERA-40 precipitation forecasts? This question is addressed by splitting the composites discussed in section 6a into hits, misses, and false alarms (section 6b). 3) Are cases of misforecasts related to problems with predicting the synoptic-scale setting and/or problems with the mesoscale precipitation generation? This question is addressed with composites of differences between ERA-40 60-h forecasts and corresponding ERA-40 reanalysis fields (section 6c). Some results in this section are illustrated with short discussions of exemplary cases.
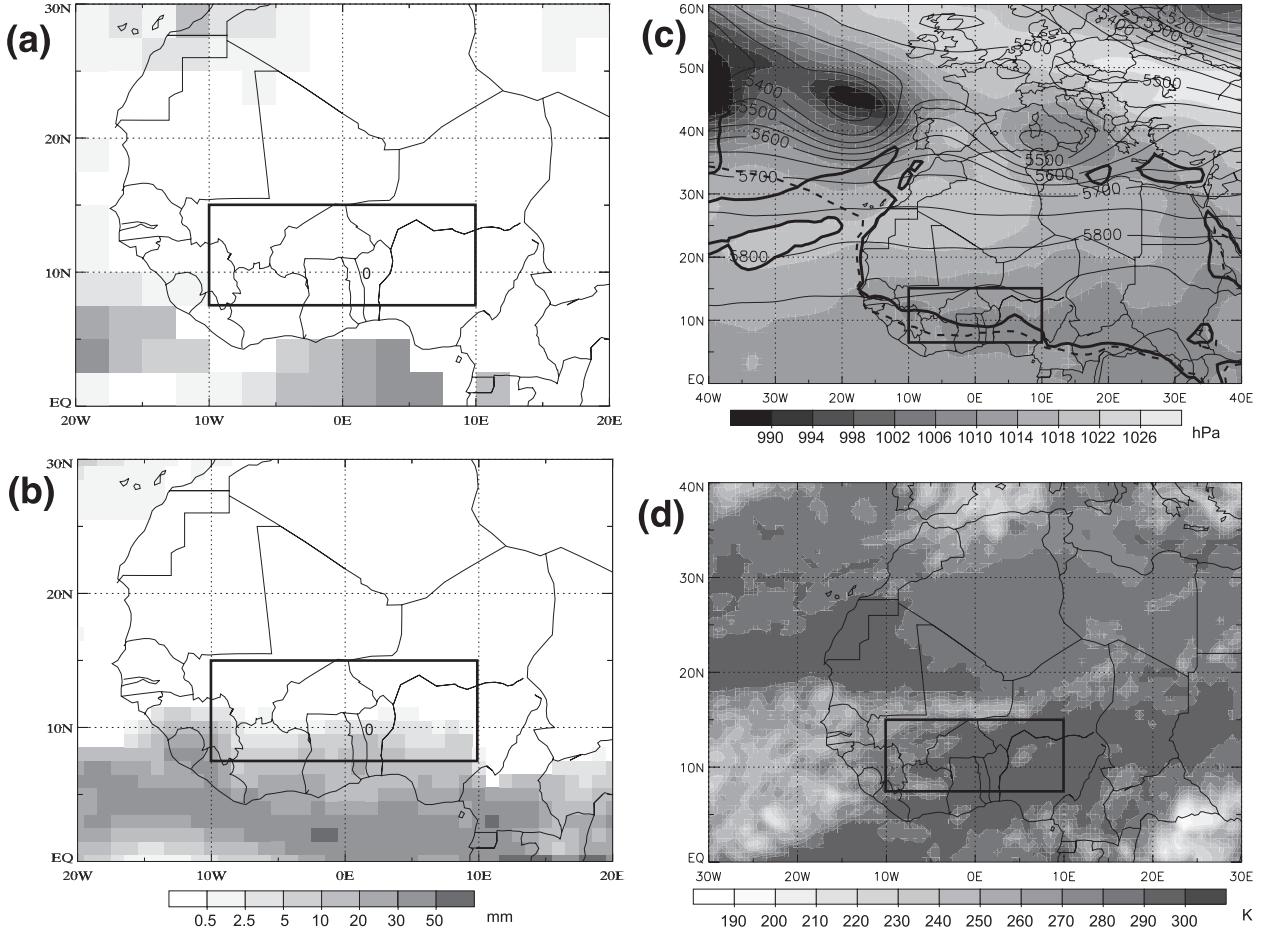
FIG. 10. Example of an extreme false alarm. The 5-day accumulated precipitation during the pentad 6–10 Jan 1997 (mm) from (a) ERA-40 forecast data and (b) GPCP. Only the synoptic station Djougou reported traces of precipitation during this period. (c) Analyzed Z500 (contours every 50 gpm), MSLP (shading), and 14°C contour of TD2M (thick solid line) at 1200 UTC 7 Jan 1997. The dashed line shows the 1979–2002 January average of the latter contour as a reference. (d) CLAUS IR BTs at 2100 UTC 7 Jan 1997. Black boxes mark the study area.

a. The typical evolution of a wet event

For all 43 wet events Fig. 11 shows composite evolutions in Z500, MSLP, TD2M, and CLAUS BTs for day −8, day −5, day −2, and day +1, with day 0 being the center of the pentad. Displayed are anomalies in the ERA-40 reanalysis fields with respect to long-term monthly means. Only 1200 UTC values of Z500, MSLP, and TD2M were considered, while the full 3-hourly resolution was used for the BT composites. Already 6 days before the beginning of the precipitation pentad, that is, on day −8, a marked signal in both Z500 and MSLP is found (Fig. 11a). The Z500 field shows a tripole with positive anomalies to the northwest of the British Isles, negative values stretching from northwestern Africa to Russia, and finally a weakly positive anomaly centered over the Libyan coast. The negative anomaly has a structure consistent with the upper trough shown

in Fig. 2a. An inspection of the 43 single cases reveals that despite the rather strong signal the spread between individual members is large with 13 cases even having positive anomalies over northwestern Africa (not shown). The MSLP signal indicates a largely barotropic structure with negative anomalies of more than 5 hPa over the Mediterranean Sea. The area with reduced MSLP stretches as far south as northern Nigeria with only weak impacts on the low-level moisture field at this stage. The CLAUS BT anomalies (Fig. 11b) are positive to the southwest of the upper trough, where subsidence and cloud breakup is expected, and negative to the southeast, where TP occurrence is expected (cf. Fig. 2b). McGuirk and Ulsh (1990) already documented such dry–wet dipoles in connection with TPs. Unusually cold cloud tops are also found in the area of largest negative Z500 anomalies and over the Gulf of Guinea, the Guinea coast, and the southern part of the study area,
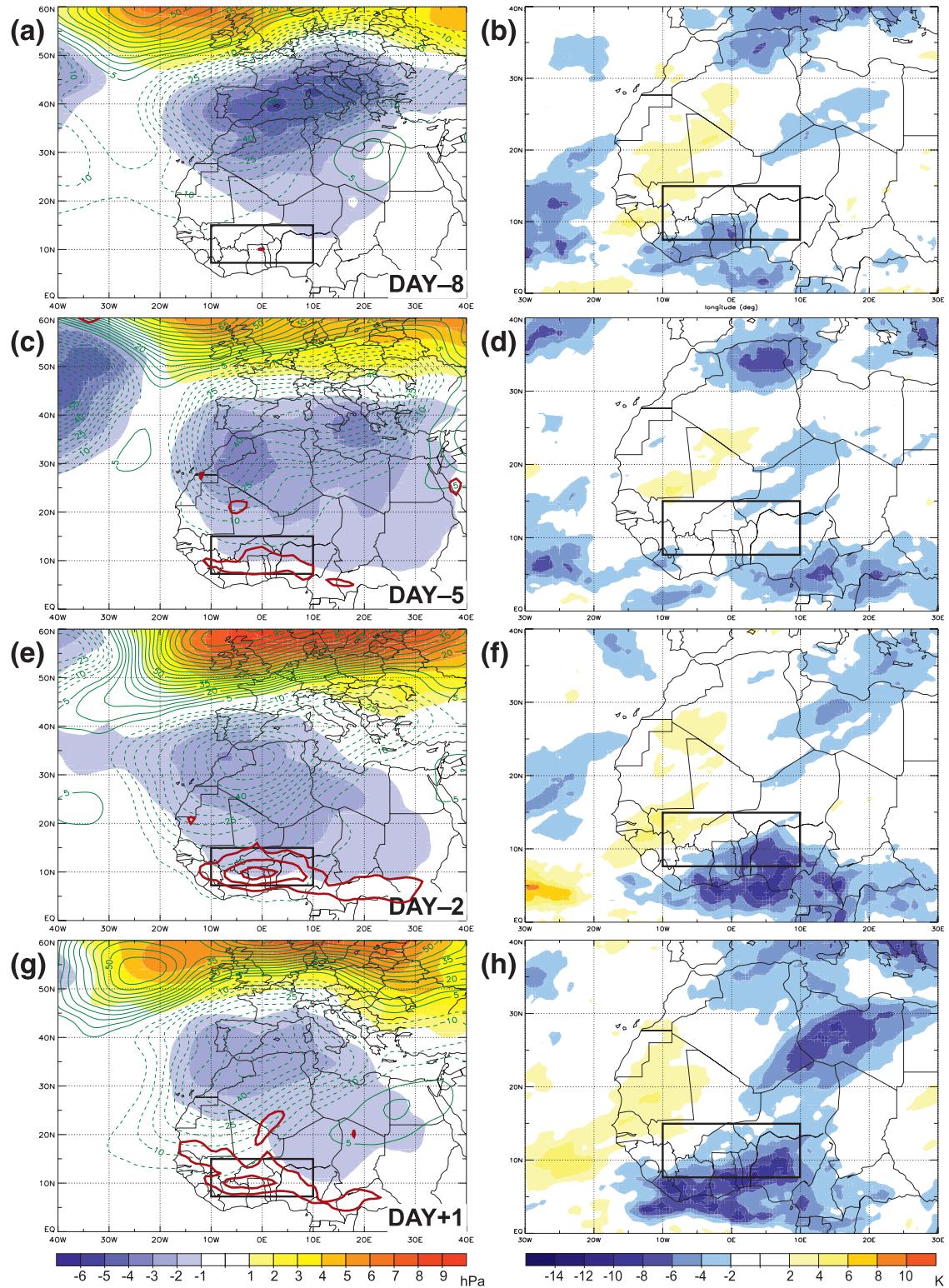
FIG. 11. Composited anomalies of (left) Z500 (green contours every 5 gpm), MSLP (shaded), and TD2M (red contours showing 2°, 4°, and 6°C) as well as (right) CLAUS IR BTs over all 43 wet events identified in section 4b for (a),(b) day −8, (c),(d) day −5, (e),(f) day −2, and (g),(h) day +1. No CLAUS data are available before 1983, so these composites consist of only 35 events. Black boxes mark the study area. Note the different geographical areas in the right and left panels.

suggesting anomalous rainfall related to the reduced MSLP and marginally enhanced moisture over the continent.

Over the next 3 days the upper trough and surface low move eastward to the Ionian Sea, while a new barotropic disturbance approaches northwest Africa from the west (Fig. 11c). Together the two disturbances create a region of negative MSLP anomalies covering almost the entirety of North Africa from the Mediterranean coast to the Sahel. This allows the ITD to move northward as indicated by the positive TD2M anomalies over the study region. The lowest absolute MSLP in the tropics is now farther to the east (not shown) and precipitation appears to be enhanced over Cameroon and the Central African Republic (Fig. 11d). There are also anomalously cold cloud tops over the Algerian and Tunisian Atlas, to the east of the western MSLP anomaly.

Another 3 days later, on day −2, the eastern disturbance has decayed while the western disturbance has slightly shifted southward into Africa (Fig. 11e). The positive anomalies over northern Europe found throughout the entire period are strongest, creating a pronounced north–south dipole with a strong gradient between the two centers. Z500 anomalies of −5 gpm are found over the Gulf of Guinea, while MSLP is reduced by up to 2 hPa at the northern end of the study area. This situation allows moist southerlies to penetrate into the box marked in Fig. 11, as indicated by the TD2M anomalies of as high as 7°C (Fig. 11e). This increase in moisture feeds the unusual dry-season precipitation over the next 4 days. The low Z500 over the tropics indicates a reduced vertical stability that also favors deep convection. This is consistent with the widespread negative BT anomalies reaching from the Gulf of Guinea far into the study area, particularly over Nigeria (Fig. 11f). Finally, by day +1 the disturbance over northwest Africa has begun to weaken and to move northeastward (Fig. 11g). Interestingly, the anomaly pattern resembles day −8 with a weaker disturbance over the Mediterranean Sea (Fig. 11a). The TD2M and BT anomaly patterns, however, strongly differ in magnitude with anomalous low-level moisture and very cold cloud tops over the study region, a clear TP centered over Libya, and warm anomalies over Mauritania and the adjacent Atlantic (Fig. 11h). These differences suggest that it is not the strength of the extratropical disturbance alone that matters for the tropical rainfall enhancement, but the whole evolution with a previous disturbance preconditioning the tropics through poleward moisture transports as discussed by Knippertz and Martin (2005). After day +2, the extratropical disturbance rapidly weakens (not shown).

This composite analysis corroborates a connection between dry-season wet events in tropical West Africa with extratropical disturbances penetrating to very low latitudes. The strong signal in Z500 and MSLP almost a week before the unusual precipitation event is remarkable and suggests the importance of a succession of two extratropical disturbances. The rather weak indications of a TP from day −8 to day −2 (Figs. 11b, 11d, and 11f) suggest that, in a statistical sense, the diabatic mechanism of pressure reduction found by KF08 is probably less important than its dynamic counterpart related to warm advection. The stronger TP signals for day −1 (not shown), day 0 (Fig. 12b), and day +1 (Fig. 11h) point to the possible importance for later stages of the evolution.

b. Influence of the dynamics on the quality of the precipitation forecast

In Figs. 12a and 12b the same composites as in Fig. 11 are shown for day 0. They largely resemble the ones for day +1 (Figs. 11g and 11h) but with a more pronounced TP and even colder cloud tops over the study area. If these results are now compared to corresponding composites for hits only, much more widespread cold cloud tops and higher low-level moisture are found in the study region, together with a somewhat stronger upper-level trough and a much clearer warm–cold dipole in the BT anomalies, that is, a much clearer TP, while the MSLP signal is very similar (Figs. 12c and 12d). This suggests that events with a large-scale organization and a clear link to the extratropics are reliably reproduced. Composites for all misses have a markedly different structure. The Z500 and MSLP signals show two barotropic disturbances, one to the west of the Iberian Peninsula and one over Tunisia and the Gulf of Gabes (Fig. 12e), that do not reach as far into the tropics as for the hits and therefore cause a weaker northward moisture advection as is evident from the smaller TD2M anomalies (cf. Figs. 12c and 12e). Negative BT anomalies are analyzed to the east of the two disturbance centers and a TP stretches along their southern flanks from off of the Senegalese coast to eastern Libya (Fig. 12f). In the study region there are scattered localized negative BT anomalies, but the signal is comparably weak and has no evident connection to the extratropics. This result appears consistent with frequent forecast misses in November (see section 5b).

These results can be illustrated with the forecast miss during the 31 January–4 February 1998 pentad. At 1200 UTC 2 February the Z500 and MSLP distributions (Fig. 13a) show a strong disturbance to the west of the Iberian Peninsula and a weak trough over the eastern Mediterranean consistent with the composite in Fig 12e.
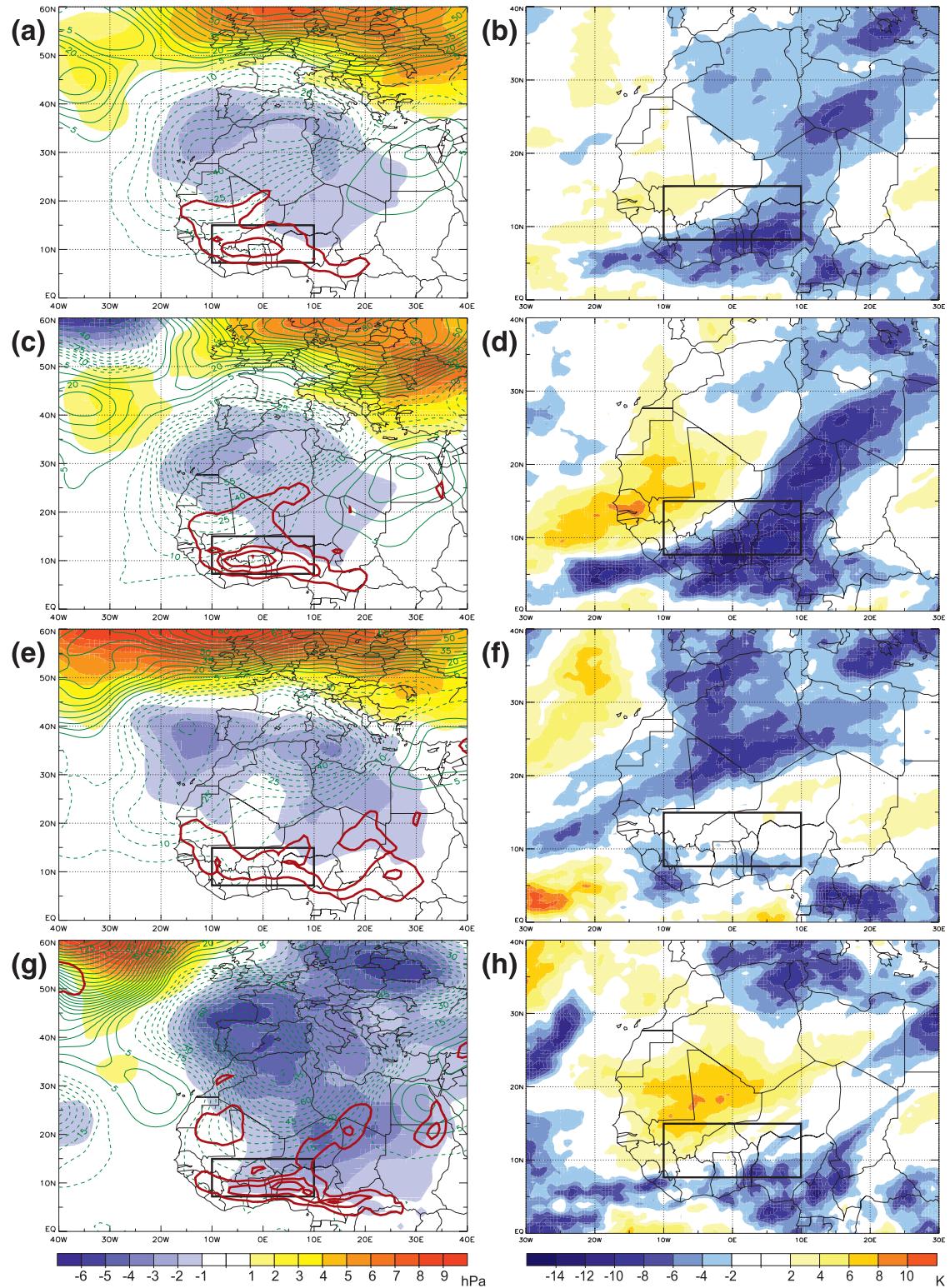
FIG. 12. Composited anomalies of (left) analyzed Z500 (contoured every 5 gpm), MSLP (shaded), and TD2M (red contours showing 2°, 4°, 6°, and 8°C) as well as (right) CLAUS BTs for day 0 over (a),(b) all 43 wet events, (c),(d) all 23 hits, (e),(f) all 20 misses, and (g),(h) all 11 false alarms. No CLAUS data are available before 1983, so these composites consist of (b) 35 events, (d) 20 events, and (f) 15 events. The false alarms are not affected. Black boxes mark the study area. Note the different geographical areas in the right and left panels.
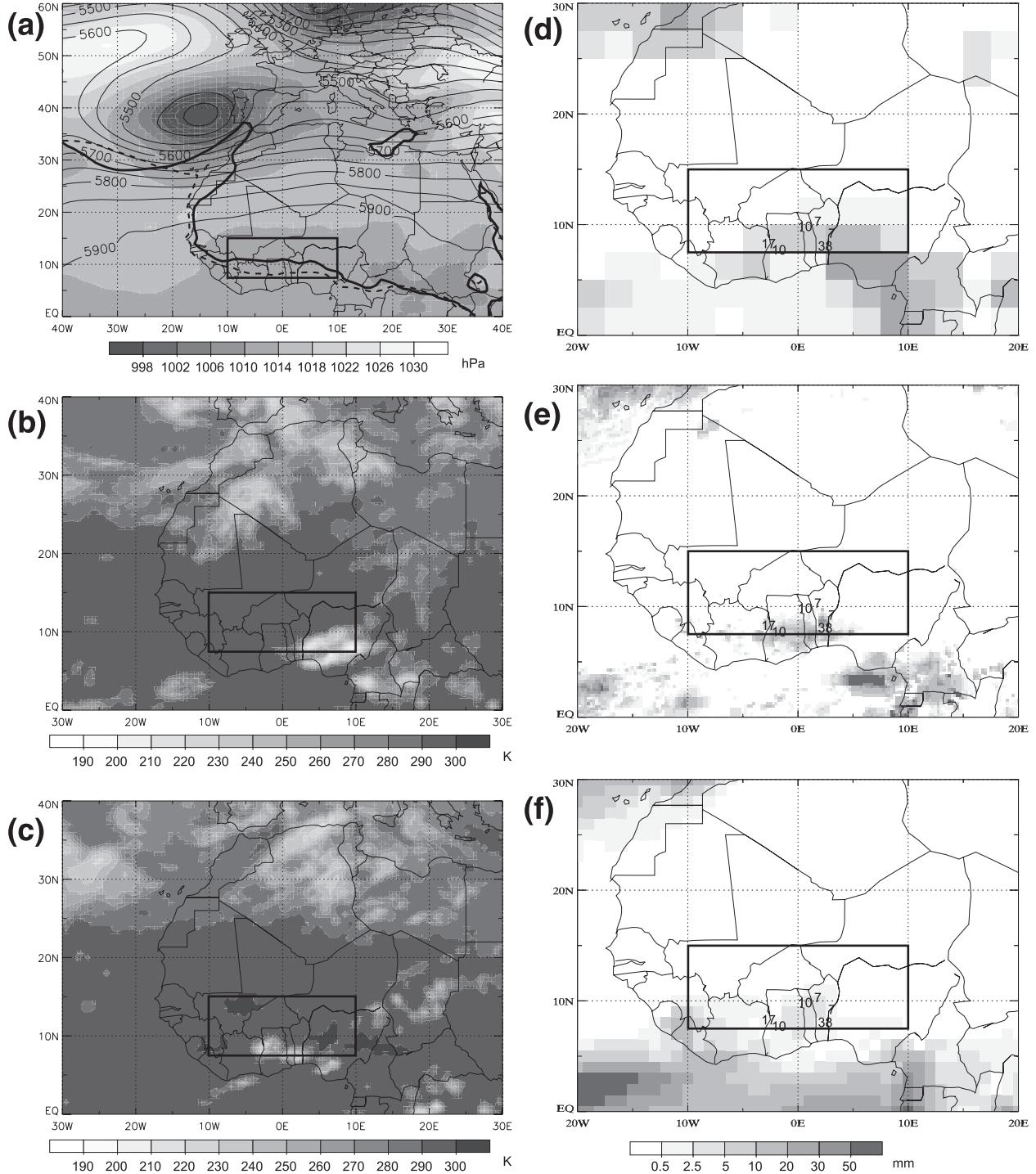
FIG. 13. Example of a forecast miss. (a) Analyzed Z500 (contours every 50 gpm), MSLP (shading), and 14°C contour of TD2M (thick solid line) at 1200 UTC 2 Feb 1998. The dashed line shows the 1979–2002 February average of the latter contour as a reference. (b),(c) CLAUS IR BTs at 2100 UTC on 1 and 2 February, respectively. (d)–(f) As in Fig. 1 but for 31 Jan–4 Feb 1998. Black boxes mark the study area.

Negative MSLP anomalies are found over all of northern Africa down to about 12°N (not shown) that are associated with enhanced moisture transports into the continent (Fig. 13a). The upper trough, however, is too remote to directly influence the precipitation generation as for example during the case in February 1999 (Fig. 2a). Instead, CLAUS BT data for this period indicate precipitation generation by rather localized convective cells forming in the afternoon hours of 31 January, and of 1 and 2 February (Figs. 13b and 13c). In the GPCP data the precipitation zone penetrates into the eastern and central part of the study region, consistent with the CLAUS data and the few available station observations (Fig. 13d), leading to an area-averaged anomaly of 398%. The TRMM data show more localized precipitation over Ghana, Togo, and Benin (Fig. 13e). The disagreement between the observational datasets underlines the general difficulty of forecast evaluation in this region as discussed earlier in this paper. The ERA-40 forecasts extend the precipitation zone into the study region, but it is not widespread and not intense enough (Fig. 13f), resulting in an area-averaged anomaly of −23%. These results suggest difficulties of the ECMWF model in triggering convection in cases with an anomalous moisture inflow into the study region prior to day 0 but without a direct synoptic forcing by an upper-level trough as for the hits. The possible influence of a misforecasted synoptic setting is addressed in section 6c.

The composite analysis for the false alarm cases reveals very large anomalies in Z500, MSLP, and TD2M (Fig. 12g). Note, however, that the strength of the anomalies is strictly speaking not directly comparable to the hits and misses due to the smaller sample size. In contrast to the other cases the orientation of the Z500 anomaly is from the northwest to the southeast, leading to negative vorticity advection, subsidence, and positive BT anomalies over large parts of West Africa (Fig. 12h). The MSLP shows its strongest anomalies over the Bay of Biscay (<-5 hPa) and over northeastern Niger (<-4 hPa). The latter is associated with enhanced moisture inflow into the continent as reflected in large positive TD2M anomalies (Fig. 12g), while substantial cold BT anomalies are restricted to the southeastern corner of the study area (Fig. 12h). Possibly the strong subsidence creates a rather dry and stable midtroposphere with capping inversions, which is not conducive for deep convection, even in the presence of low-level moist air. It is conceivable that the ECMWF model struggles to capture such stable layers and therefore forecasts too much precipitation in these situations. A thorough investigation of this idea would require a detailed comparison with available radiosonde data,

which is beyond the scope of this paper. Possible other reasons are an underestimation of precipitation in the GPCP data, for example, due to a lack of surface observations or a mispredicted synoptic setting. The first hypothesis cannot be tested without an additional independent source of information to evaluate the GPCP data. The second hypothesis will be addressed in the next section.

c. Predictions of the synoptic setting

For this analysis, ERA-40 forecasts of Z500, MSLP, and TD2M started at 0000 UTC of day −2 of the respective pentad and then run for 60 h until 1200 UTC on day 0 are compared to the corresponding ERA-40 reanalyses in the form of composites for all events, all hits, all misses, and all false alarms as in Fig. 12. For all wet events the ERA-40 forecasts reveal a positive MSLP and Z500 bias over the western Mediterranean Sea and adjacent North Africa (Fig. 14a), indicating a somewhat too weak disturbance in the forecast (cf. Fig. 12a). In the tropics, Z500 and MSLP are systematically forecasted too low, consistent with a too high TD2M over the study region. If the composite is split into hits and misses, the forecast errors with respect to the large-scale circulation do not change significantly (Figs. 14b and 14c). Both hits and misses show a wet bias over the study region with the one for misses being somewhat smaller, which might explain part of why the model generates too little precipitation in these cases. The differences in the Z500 errors over the study region are presumably too small to have a substantial impact, although the positive values for the misses are at least consistent with less precipitation.

The forecast errors for false alarms have a different structure and are of larger magnitude (Fig. 14d), which again may be due to the smaller number of composite members. The most prominent signals are a TD2M error in the study region of as much as 10°C, a large northwest–southeast-oriented region with positive deviations in Z500 and MSLP stretching from the Atlantic into northwest Africa, and a region with negative values over the central Mediterranean Sea and adjacent parts of Europe. This indicates a reduction of the negative trough orientation evident from Fig. 12g in the model, which would reduce the subsidence to the southwest and south of the trough with potential positive effects on precipitation. In the tropics, however, the signals in Z500 and MSLP do not differ much from the result for all events (Fig. 14a), pointing to a rather indirect effect of these forecast errors.

To illustrate this further, Fig. 15 shows the false alarm example of 15–19 February 1991. For this period the GPCP data and station observations indicate an unusual
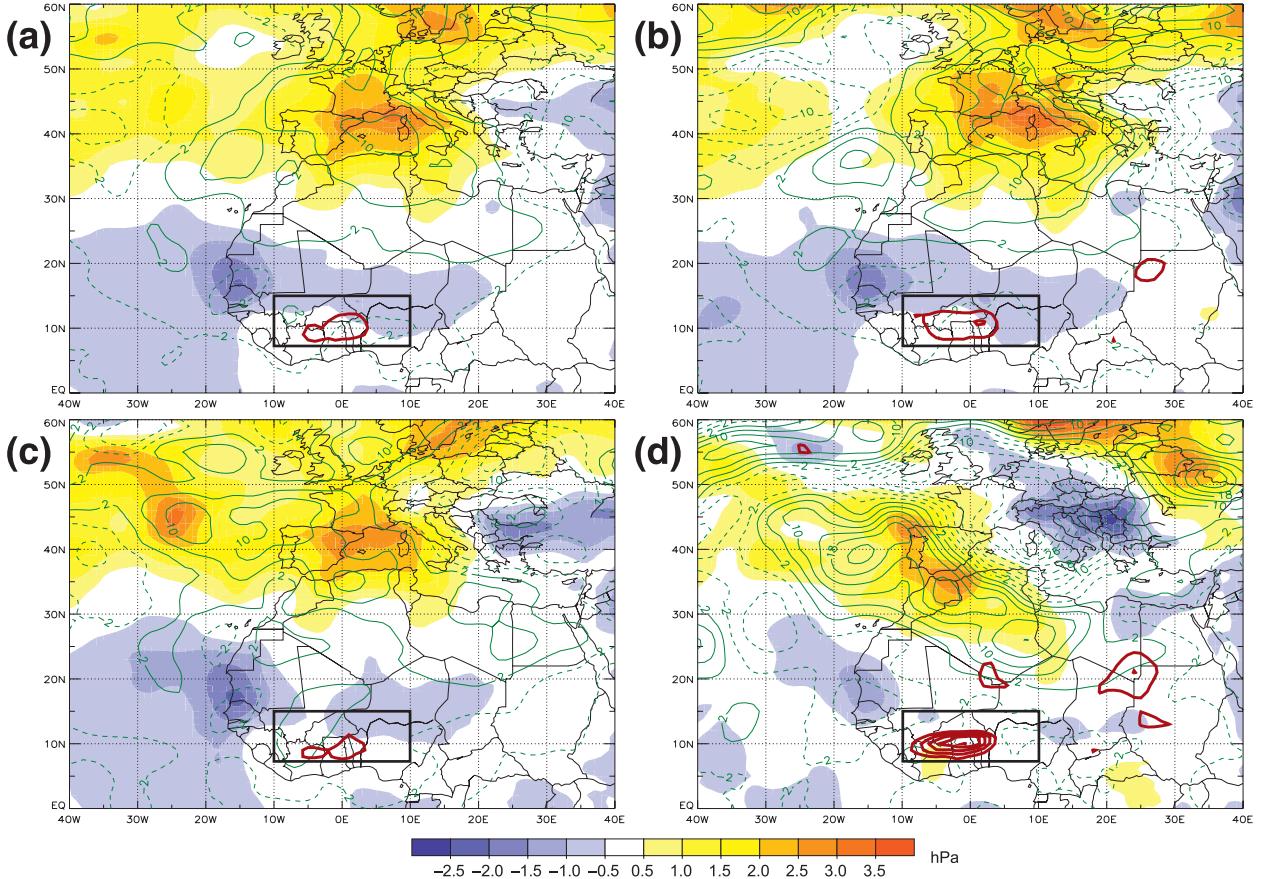
FIG. 14. Composited differences of Z500 (green contours every 4 gpm), MSLP (shaded), and TD2M (red contours showing 2°, 4°, 6°, 8°, and 10°C) between the 60-h forecasts from ERA-40 and the corresponding reanalysis for day 0: (a) all 43 wet events, (b) all 23 hits, (c) all 20 misses, and (d) all 11 false alarms. Black boxes mark the study area.

penetration of rainfalls into the study area but with rather low amounts (Fig. 15a), while the ERA-40 model forecasts more widespread and more intense rainfalls (Fig. 15b). The synoptic situation on day 0 of the pentad is characterized by a conspicuous disturbance close to the Iberian Peninsula connected to a low pressure corridor stretching from Niger to Algeria that is most likely responsible for the shift of the ITD and the rain zone into the study region (Fig. 15c). These patterns closely agree with the false alarm composite shown in Fig. 12g. Consistent with Fig. 14d, the forecast errors are comparably large, reaching positive values in Z500 of more than 60 gpm over the Atlantic and Algeria, and negative values of the same magnitude over the western Mediterranean Sea (Fig. 15d). Corresponding to the upper-level patterns, maximum MSLP errors are as large as +11 hPa over the Portuguese coast and −4 hPa over northeastern Spain. These errors shift the disturbance center from the western to the eastern side of the Iberian Peninsula and lead to a more positive tilt of the upper-level trough and slightly lower MSLP in a band

stretching from Guinea to Libya. The latter is consistent with the positive TD2M errors and stronger precipitation in the model. Interestingly, there is also a pronounced positive TD2M error close to the border triangle area of Algeria–Mali–Niger (Fig. 15d). In conclusion, these results suggest that the false alarms are to some degree related to worse forecasts of the large-scale circulation, in particular of the moisture distribution in the tropics and the orientation of the trough axis in the subtropics, which determines the vertical motion patterns. In addition, problems with the precipitation generation, specifically with the suppression of deep convection through capping inversions, and also with the quality of the observations cannot be ruled out.

7. Summary and conclusions

Precipitation events during the heart of the dry season in tropical West Africa from November to February are rare, but can have significant impacts locally. Previous work has suggested a link to upper-level troughs from
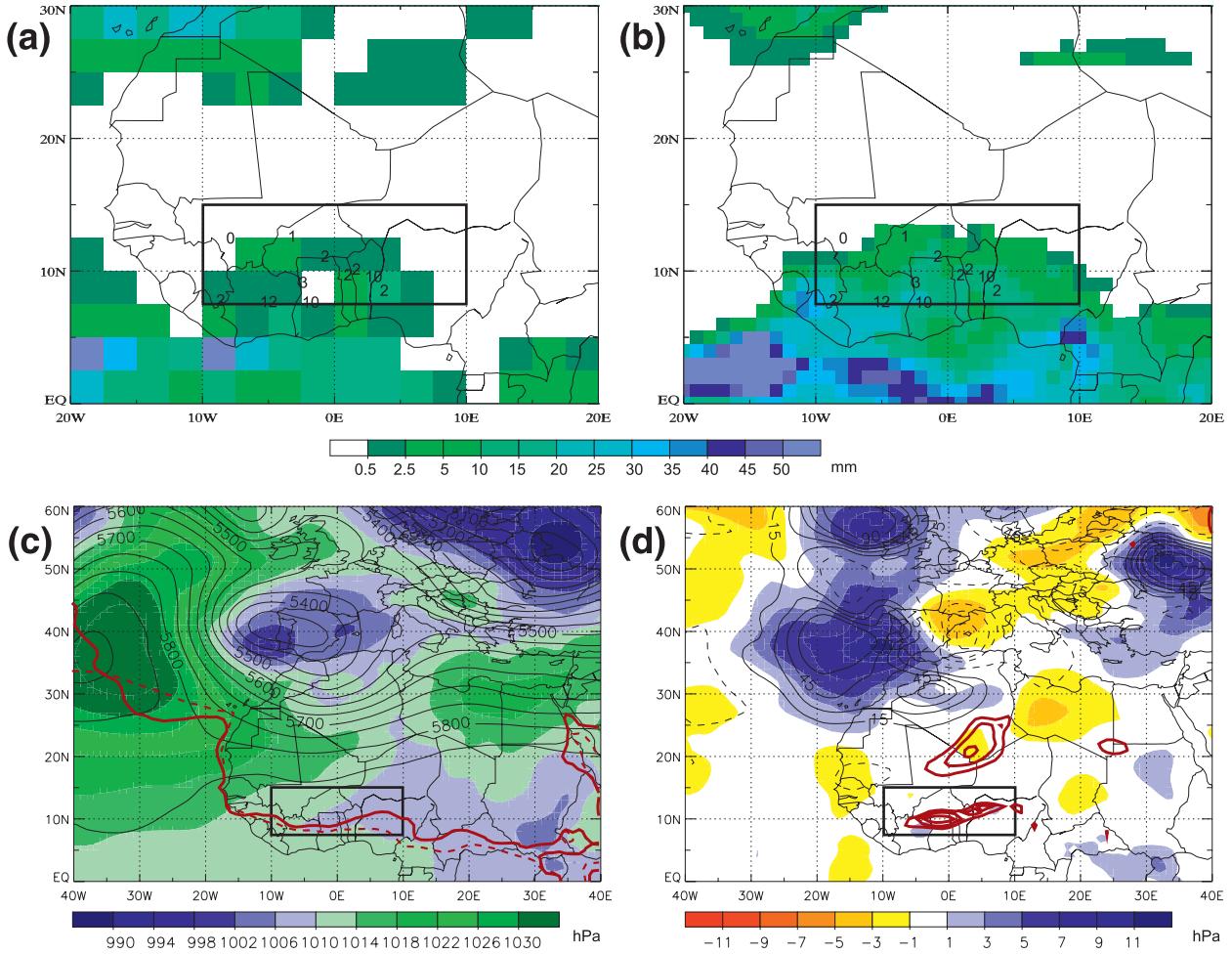
FIG. 15. Example of a false alarm. (a),(b) As in Figs. 1a and 1c but for 15–19 Feb 1991. (c) Z500 (contours every 50 gpm), MSLP (shading), and 14°C contour of TD2M (red solid line) at 1200 UTC 17 Feb 1991. The dashed red line shows the 1979–2002 February average of the latter contour as a reference. (d) Differences of Z500 (contoured every 15 gpm), MSLP (shaded), and TD2M (red contours showing 6°, 10°, and 14°C) between the 60-h forecast from ERA-40 valid at 1200 UTC 17 Feb 1991 and the corresponding reanalysis. Black boxes mark the study area.

the extratropics and a comparably high predictability of such events (KF08), which is potentially of great benefit to the local population. Here, an identification routine for such dry-season wet events was developed based on 23 winter seasons from the GPCP merged satellite–gauge pentad dataset. The algorithm uses an area-averaged (7.5°–15°N, 10°W–10°E) threshold of +200% anomaly relative to the mean seasonal cycle, resulting in an identification of 1.87 events per winter on average, with a range from zero to five. Most events occur in December and January when the absolute exceedence thresholds are lowest. A composite analysis revealed that the unusual precipitation is in fact connected to distinct upper-level disturbances in the subtropics and an associated lowering of the MSLP over the Sahara that allows moist southerlies to penetrate farther than usual during

this season into the continent. The analysis also points to the impact of low-level moisture inflow connected to a preconditioning prior disturbance about 1 week before the actual precipitation event in agreement with a case study by KF08. For extreme precipitation events in regions closer to the West African west coast, Knippertz and Martin (2005) also found a preconditioning through midtropospheric moisture advection from the deep tropics ahead of a precursor upper-level trough. This general behavior of a several-day-long moistening of the seasonally dry troposphere may help African forecasters in their day-to-day operations by anticipating the potential for high-impact weather events as early as possible. The actual wet events are accompanied by TPs to the east of the upper troughs and by unusual precipitation patterns at the northern and western fringes

of the Sahara, as already documented by KF08. With respect to the dynamical concept developed on a case study basis by KF08, the statistical results presented here suggest that the pressure fall over the Sahara is mainly related to adiabatic warm advection to the southeast of the upper trough and to a lesser degree by diabatic warming under the TP due to an increased greenhouse effect. The latter may be important in the later stages of the evolution or in transition season cases when warm advection and vertical motions associated with the troughs are weaker.

The evaluation of 5-day precipitation forecasts from the ERA-40 reanalysis dataset led to the following conclusions: (a) There is an overall wet bias in the model over the study region. (b) The temporal correlation of area averages to GPCP is highly significant with 0.77. (c) The number of wet events is underpredicted leading to a bias of 0.79 and a hit rate of 0.53 with the strongest 10 events all being well reproduced. (d) The false alarm ratio is only 0.32, indicating an overall moderate level of skill in the 5-day forecasts [in contrast to many other tropical precipitation systems, e.g., Montmerle et al. (2006)], which even increases in the later half of the study period. (e) Typical hits are characterized by a deep penetration of the extratropical disturbance into West Africa, a distinct TP, and a large-scale organization of convection in the tropics through the pronounced trough. (f) Typical misses are characterized by a northward-shifted moist zone without a deep penetration of extratropical disturbances. The abundance of low-level moisture favors the development of localized convective cells in the course of the day that are apparently less reliably reproduced by the ECMWF model. (g) Typical false alarms show a more negative orientation of the extratropical disturbance, strong subsidence over large parts of West Africa, and enhanced cloudiness over the eastern part of the study region. Possible reasons for the too strong precipitation in the ECMWF model forecasts are too moist low levels, problems with the suppression of deep convection through capping inversions in the subsidence zone and/or a more positively tilted trough orientation in the subtropics. These results corroborate the hypothesis of KF08 that a strong extratropical influence generally enhances the quality of the predictions in the tropics. In our view the presented results are promising enough to be taken advantage of by national weather services in West Africa.

One problem evident from this study is the, at times, questionable quality of the coarse resolution GPCP data used for forecast evaluation related to the sparse gauge network in West Africa (see Yin et al. 2004). Therefore, the authors intend to repeat some of the investigations presented here with the high-resolution,

high quality TRMM data available for 1998–present. A comparison of this dataset to the state-of-the-art ERA interim reanalysis would allow a further exploration of the impact of a more-refined assimilation system on forecast improvements. Moreover, spatial correlations could be considered instead of area averages to allow a more regional evaluation that is of more practical use. It would also be interesting to include extratropical influences during the post- and premonsoon seasons, that is, during October, March, and April. Another aspect raised but not entirely clarified in this and previous studies is the mechanism of preconditioning by a prior disturbance. Possible hypotheses are that an enhancement of soil moisture or a moister midtroposphere improves conditions for subsequent rainfalls.

REFERENCES

Adler, R. F., and Coauthors, 2003: The version 2 Global Precipitation Climatology Project (GPCP) monthly precipitation analysis (1979–present). *J. Hydrometeor.,* **4,** 1147–1167.

Borgne, J. L., 1979: Un exemple d'invasion polaire sur la région mauritano-sénégalaise. *Ann. Géograph.,* **489,** 521–548.

Buckle, C., 1996: *Weather and Climate in Africa.* Longman, 312 pp.

Fall, S., D. Niyogi, U. C. Mohanty, and A. Kumar, 2007: Application of weather prediction models for hazard mitigation planning: A case study of heavy off-season rains in Senegal. *Nat. Hazards,* **41,** 227–243.

Frei, C., J. H. Christensen, M. Déqué, D. Jacob, R. G. Jones, and P. L. Vidale, 2003: Daily precipitation statistics in regional climate models: Evaluation and intercomparison for the European Alps. *J. Geophys. Res.,* **108,** 4124, doi:10.1029/2002JD002287.

Gaye, A. T., S. Fongang, A. Garba, and D. Badiane, 1994: Study of Heug rainfall in Senegal using conventional data and Meteosat imagery. Ministère de la Coopération–ORSTOM–Météo-France, Veille Climatique Satellitaire, Lannion, France, 61–71.

Griffiths, J. F., 1972: Semi-arid zones. *World Survey of Climatology*, H. E. Landsberg, Ed., Elsevier, 193–210.

Hagemann, S., K. Arpe, and L. Bengtsson, 2005: Validation of the hydrological cycle of ERA-40. ERA-40 Project Report Series 24, ECMWF, Reading, United Kingdom, 42 pp.

Hodges, K., D. W. Chappell, G. J. Robinson, and G. Yang, 2000: An improved algorithm for generating global window brightness temperatures from multiple satellite infrared imagery. *J. Atmos. Oceanic Technol.,* **17,** 1296–1312.

Huffman, G. J., R. F. Adler, S. Curtis, D. T. Bolvin, and E. J. Nelkin, 2007: Global rainfall analyses at monthly and 3-hr time scales. *Measuring Precipitation from Space: EURAINSAT and the Future*, V. Levizzani, P. Bauer, and F. J. Turk, Eds., Springer-Verlag, 291–306.

Issar, A. S., 1995: Impacts of climate variations on water management and related socio-economic systems. SC.95/WS.26, Technical Documents in Hydrology, International Hydrological Programme, UNESCO, Paris, France, 97 pp.

Kållberg, P., P. Berrisford, B. Hoskins, A. Simmons, S. Uppala, S. Lamy-Thépaut, and R. Hine, 2005: *ERA-40 Atlas*. ERA-40 Project Report Series 19, ECMWF, Reading, United Kingdom, 191 pp.

Knippertz, P., 2005: Tropical–extratropical interactions associated with an Atlantic tropical plume and subtropical jet streak. *Mon. Wea. Rev.,* **133,** 2759–2776.

——, and J. E. Martin, 2005: Tropical plumes and extreme precipitation in subtropical and tropical West Africa. *Quart. J. Roy. Meteor. Soc.,* **131,** 2337–2365.

——, and A. H. Fink, 2008a: Dry-season precipitation in tropical West Africa and its relation to forcing from the extratropics. *Mon. Wea. Rev.,* **136,** 3579–3596.

——, and ——, 2008b: Rainfall events during the West African dry-season: Forcing from the extratropics and predictability. Preprints, *28th Conf. on Hurricanes and Tropical Meteorology,* Orlando, FL, Amer. Meteor. Soc., 3C.7.

Leroux, M., 2001: *The Meteorology and Climate of Tropical Africa*. Springer, 493 pp.

Mason, I. B., 2003: Binary events. *Forecast Verification. A Practitioner's Guide in Atmospheric Science,* I. T. Jolliffe and D. B. Stephenson, Eds., Wiley, 37–76.

McGuirk, J. P., and D. J. Ulsh, 1990: Evolution of tropical plumes in VAS water vapor imagery. *Mon. Wea. Rev.,* **118,** 1758–1766.

Mecikalski, J. R., and G. J. Tripoli, 1998: Inertial available kinetic energy and the dynamics of tropical plume formation. *Mon. Wea. Rev.,* **126,** 2200–2216.

Meier, F., and P. Knippertz, 2009: Dynamics and predictability of a heavy dry-season precipitation event over West Africa—Sensitivity experiments with a global model. *Mon. Wea. Rev.,* **137,** 189–206.

Montmerle, T., J.-P. Lafore, L. Berre, and C. Fischer, 2006: Limited-area model error statistics over western Africa: Comparisons with midlatitude results. *Quart. J. Roy. Meteor. Soc.,* **132,** 213–230.

Seck, A., 1962: Le Heug ou pluies de saison sèche au Sénégal. *Ann. Géograph.,* **385,** 225–246.

Uppala, S. M., and Coauthors, 2005: The ERA-40 re-analysis. *Quart. J. Roy. Meteor. Soc.,* **131,** 2961–3012.

Xie, P., and P. A. Arkin, 1997: Global precipitation: A 17-year monthly analysis based on gauge observations, satellite estimates, and numerical model outputs. *Bull. Amer. Meteor. Soc.,* **78,** 2539–2558.

——, J. E. Janowiak, P. A. Arkin, R. F. Adler, A. Gruber, R. R. Ferraro, G. J. Huffman, and S. Curtis, 2003: GPCP pentad precipitation analyses: An experimental dataset based on gauge observations and satellite estimates. *J. Climate,* **16,** 2197–2214.

Yin, X., A. Gruber, and P. Arkin, 2004: Comparison of the GPCP and CMAP merged gauge–satellite monthly precipitation products for the period 1979–2001. *J. Hydrometeor.,* **5,** 1207–1222.